Technical note: Identification of chemical composition and source of fluorescent components in atmospheric water-soluble brown carbon by excitation-emission matrix with parallel factor analysis: Potential limitation and application

Tao Cao[1,2,3], Meiju Li[1,2,3], Cuncun Xu[1,2,3], Jianzhong Song[1,2,5,*], Xinjun Fan[4], Jun Li[1,2,5], Wanglu Jia[1,2], Ping'an Peng[1,2,3,5]

[1]State Key Laboratory of Organic Geochemistry and Guangdong Provincial Key Laboratory of Environmental Protection and Resources Utilization, Guangzhou Institute of Geochemistry, Chinese Academy of Sciences, Guangzhou 510640, China

[2]CAS Center for Excellence in Deep Earth Science, Guangzhou 510640, China

[3]University of Chinese Academy of Sciences, Beijing 100049, China

[4]College of Resource and Environment, Anhui Science and Technology University, Fengyang 233100, China

[5]Guangdong-Hong Kong-Macao Joint Laboratory for Environmental Pollution and Control, Guangzhou 510640, China

Correspondence to: Jianzhong Song, E-mail: songjzh@gig.ac.cn.

Abstract

Three-dimensional excitation-emission matrix (EEM) fluorescence spectroscopy is an important method for the identification of occurrences, chemical compositions, and sources of atmospheric chromophores. However, current knowledge on the identification and interpretation of fluorescent components is mainly based on aquatic dissolved organic matter and might not be applicable to atmospheric samples. Therefore, this study comprehensively investigated EEM data of different types of strong light-absorbing organic compounds, water-soluble organic matter (WSOM) in different aerosol samples (combustion source samples and ambient aerosols), soil dust, and purified fulvic and humic acids supplemented by parallel factor (PARAFAC) modelling. The results demonstrated that organic compounds with high aromaticity and strong electron-donating groups generally present strong fluorescence spectra at longer emission wavelengths, whereas organic compounds substituted with electron-withdrawing groups have relatively weaker fluorescence intensity. In particular, aromatic compounds containing nitro groups (i.e., nitrophenols), which show strong absorption and are the major component of atmospheric brown carbon, exhibited no significant fluorescence. EEM-PARAFAC identified three fluorescent components (i.e., C1, C2, and C3) in ambient WSOM. Although EEM-PARAFAC derived C1 (235, 270/330 nm) in ambient WSOM is generally considered as protein-like groups, our findings suggested that it is mainly composed of aromatic acids, phenolic compounds, and their derivatives, with only traces of amino acids. C2 is associated with the atmospheric chemical reaction of

biomass burning and/or biogenic organic molecules, with relatively lower degree of oxidation, which are more abundant in Guangzhou WSOM (56%-69%). Whereas, C3 is mainly attributed to highly oxygenated organic molecules derived from soil and atmospheric aging processes and has a relatively higher contribution in Chuzhou WSOM (23%). These findings provide new insights for the analysis of chemical properties and sources of atmospheric fluorophores using the EEM method.

1. Introduction

Water-soluble organic carbon (WSOC) constitutes a substantial fraction (10–80%) of organic aerosols in the atmosphere and is ubiquitous in ambient aerosols, clouds or fog, and rain water (Wozniak et al., 2012; Huang et al., 2022, Zhang et al., 2022a). Recent studies have highlighted that a portion of WSOC, termed brown carbon (BrC), can absorb light in the near-ultraviolet and visible ranges (Laskin et al., 2015, Frka et al., 2022; Ma et al., 2022). Owing to its strong light-absorption capacity, BrC can cause up to 45% solar radiation absorption by atmospheric aerosols and has potential effects on regional and even global climate (Zhang et al., 2013). In addition, BrC also participates in atmospheric photochemical reactions, affects the physicochemical properties of atmospheric aerosols (Laskin et al., 2015; Tang et al., 2020b), and potentially, can be activated to form reactive oxygen species that cause adverse effects on human health (Cao et al., 2021; Zhang et al., 2022b).

Excitation-emission matrix (EEM) fluorescence spectroscopy is a highly sensitive and widely used analytical technique for the identification of chemical

characteristics and sources of chromophores in dissolved organic matter (DOM) in aquatic environments (Murphy et al., 2010, 2013; Zhang et al., 2014). Recently, EEM has been further extended and frequently applied for the investigation of water-soluble organic matter (WSOM), such as light-absorbing organic compounds in atmospheric aerosols and fine particles from combustion processes (Chen et al., 2020; Fan et al., 2016; Wu et al., 2020; Yang et al., 2022). For instance, humic-like substances (HULIS) and protein-like substances (PRLIS) have been identified as important fluorescent components in combustion-derived particles (Cao et al., 2021; Tang et al., 2021) and ambient aerosols (Ma et al., 2022; Wu et al., 2020; Yang et al., 2022). Chen et al. (2016) used EEM coupled with parallel factor analysis (PARAFAC) and high-resolution mass spectrometry to identify chromophores in ambient aerosols and proposed that fluorescent components with longer excitation (Ex)/emission (Em) wavelengths comprise more highly oxygenated groups (Chen et al., 2016a). In addition, further application of the EEM method has also revealed that the concentration and types of fluorophores obviously vary during atmospheric processes, such as photolytic aging of biomass burning (BB)-derived chromophores (Aftab et al., 2018; Tang et al., 2020b). Therefore, the EEM method has significant potential for the characterization (types, sources, and evolution) of atmospheric BrC.

However, application of the EEM method for the identification of atmospheric BrC has some limitations. It is well known that the present identification, classification, and interpretation of fluorescent components in atmospheric WSOM are mainly based on the fluorescence peak position of DOM in aquatic environments

(Coble, 1996; Wünsch et al., 2019). Nonetheless, the chemical and molecular composition and source of WSOM in atmospheric aerosols significantly vary from those of DOM in aquatic environments (Graber and Rudich, 2006; Laskin et al., 2015); hence, the current fluorescence criterion derived from aquatic environments could lead to some inaccurate description of the fluorescent components in atmospheric WSOM. For instance, the EEM region at Ex/Em = 235(270)/330 nm is assigned to PRLIS and/or tryptophan-like substances in aquatic environments (Coble, 1996), but is also associated with non-nitrogen species such as polyphenols in atmospheric WSOM (Chen et al., 2016b). The EEM region at peak M (290–315/370–420 nm) is considered as a typical signal of marine-derived HULIS (Coble, 2007; Zhao et al., 2019), but the source of this peak should be cautiously investigated when interpreting BrC in continental aerosols. In addition, the intensities of fluorescent species are not always linearly correlated with their concentrations, which can be affected by the aromatic ring system and the number and types of functional groups, thereby leading to greater uncertainty in intensity measurements (Andrade-Eiroa et al., 2013; Chen et al., 2020; Wang et al., 2020). Atmospheric BrC is composed of complex organic molecules with different light absorption properties (Lin et al., 2020; Huang et al., 2021; Jiang et al., 2022), and only a subset of BrC molecules that contain functional groups are capable of fluorescence emission upon relaxation from an excited state (Andrade-Eiroa et al., 2013). Hence, interpretation of fluorescence data may only correspond to fluorescent chromophores and may not be representative of BrC as a whole (Chen et al., 2020;

107 Wang et al., 2020). All these factors limit further application of the EEM method for

108 the analysis of atmospheric BrC. Therefore, it is essential to investigate the

109 light-absorbing species that can be detected by EEM and obtain important

110 information for identifying the chemical compositions and possible sources of these

111 species.

112 Accordingly, in the present study, the EEM profiles of a series of BrC model

113 compounds and WSOM isolated from primary combustion samples, soils, and

114 atmospheric aerosols were investigated. The chemical characteristics and sources of

115 the main fluorophores were interpreted according to the fluorescence peaks location

116 and intensity, and the chemical structures of the model compounds and source

117 samples were analyzed. Then, atmospheric aerosols in Guangzhou (GZ) and

118 Chuzhou (CZ) cities were collected and fluorescent chromophores within the

119 water-soluble fraction were identified to estimate the application of the

120 EEM-PARAFAC method in characterizing atmospheric BrC. The results obtained

121 help to broaden the application of the EEM-PARAFAC method to study atmospheric

122 BrC.

123

124 **2. Materials and methods**

125 2.1. Materials

126 For accurate identification of the chemical composition and structures of

127 fluorophores in atmospheric BrC and for assessment of application of the EEM

128 method to examine atmospheric BrC, a total of 136 samples were investigated in this

study. The samples comprised: (1) 35 BrC model compounds, including phenolic compounds, aromatic acids, nitroaromatic compounds (NACs), PRLIS, N-heterocyclic compounds, and polycyclic aromatic hydrocarbons (PAHs) and their derivatives (detailed information in Text S1.1 and Table S1 of supporting information (SI)). These compounds are usually detected in ambient samples and have been considered typical BrC model compounds (Frka et al., 2022, Lin et al., 2016; 2017; Wang et al., 2017; Huang et al., 2021); (2) 13 primary combustion source samples collected from BB, coal combustion (CC), and vehicle emission (VE); (3) five soil samples obtained from the rural area of Guangdong Province, China, with different vegetation, which is also an important source of atmospheric BrC and has been widely identified in previous studies (Chen et al., 2020; Vasilatou et al., 2017); (4) six purified fulvic and humic acids (FAs and HAs, respectively) kindly provided by Professor Weilin Huang (Rutgers, The State University of New Jersey, NJ, USA); and (5) 34 diurnal fine particulate matter ($PM_{2.5}$) samples collected from 6 to 22 April, 2021 at GZ and CZ, respectively. In addition, 43 annual $PM_{2.5}$ samples were collected from February 2018 to January 2019 at the GZ site and classified as wet and dry season atmospheric $PM_{2.5}$ samples (for detailed information, see Text S1 of SI). Field blank samples were collected without instrument power on during each sampling period.

2.2. Standard solution and aqueous extraction of ambient samples

Solutions of model organic compounds were prepared by dissolving a certain

151   amount of dried solid or liquid samples in Milli-Q water or methanol. The ambient

152   aerosol and soil samples were ultrasonically extracted with ultrapure water three

153   times, and the supernatants were filtered using a 0.22-μm PTFE syringe filter to

154   isolate the WSOM. The specific separation and purification methods have been

155   published in previous studies (Chen et al., 2020; Fu et al., 2015; Wang et al., 2020;

156   Yan and Kim, 2017) and are presented in the SI (Test S2).

157

158   **2.3. EEM-PARAFAC analysis**

159   The EEM fluorescence spectra of the aqueous extraction of the samples in 1-cm

160   quartz cuvettes were recorded using a three-dimensional fluorescence

161   spectrophotometer (Aqualog; HORIBA Scientific, USA) at room temperature. The

162   scanning ranges for Ex and Em were 200–500 and 250–550 nm, respectively. The

163   wavelength increment of the Ex and Em scans was 5 nm, the integration time was

164   0.5 s, and Milli-Q water (18.2 MΩ cm) used as blank reference. The absorbance

165   measurements were used to correct the EEM for inner filter effects (IFEs) as

166   described previously (Fu et al., 2015) if the absorbance was > 0.05 at 250 nm

167   (Murphy et al., 2013; Tang et al., 2020a). Background samples were also analyzed

168   and the background values were subtracted from the values obtained for all the

169   samples. To avoid concentration effects, the fluorescence spectra were normalized by

170   the water Raman area to produce Raman unit (R.U.) and further by the organic

171   carbon concentration of the samples to the normalized fluorescence intensities

172   (R.U./(mg C/L)) (Yang et al., 2022) are shown in Table S2.

173   The PARAFAC modelling procedure was conducted for 77 atmospheric WSOM

174   samples in MATLAB 2014b (Mathwork.Inc, USA) using the drEEM toolkit

175   (Murphy et al., 2018; Wünsch et al., 2019). PARAFAC was computed using two to

176   nine component models, with non-negativity constraints and residual analysis, and

177   split-half analysis was employed to validate the number of fluorescent components.

178   Based on the results of the split-half and core consistency analyses, three-component

179   models were chosen for further investigation. The relative contribution of individual

180   chromophores was estimated by calculating the maximum fluorescence intensities

181   (F_{max}: maximum fluorescence intensity of the identified fluorescent components;

182   relative content (%) = $F_{max}/\Sigma F_{max}$) (Chen et al., 2020; Fan et al., 2020).

183

184   **3. Results and discussion**

185   **3.1. Fluorescence properties of BrC model compounds**

186   To identify whether the light-absorbing species possess fluorescence, a series of

187   BrC model compounds were tested by the EEM method, and the fluorescence

188   profiles are shown in Fig. S1. The results revealed that the location and intensity of

189   the fluorescence peaks of different compounds were different, which varied with the

190   distinct functional groups and aromatic conjugate system.

191   Although phenolic compounds are important light-absorbing species in

192   atmospheric BrC (Smith et al., 2016; Yu et al., 2014, 2016), not all of them exhibit

193   strong fluorescence. As shown in Fig. S1a, a strong fluorescence peak in the EEM

194   spectrum of phenol was observed at Ex/Em = 270/295 nm. When the phenol

195   compounds were substituted with electron-donating groups (e.g., hydroxyl), all of

196   the stronger fluorescence peaks were obviously red-shifted to 310–320 nm (e.g.,

197   catechol, hydroquinone, and 2-methoxyphenol). However, phenolic compounds

198   substituted with electron-withdrawing groups (e.g., carboxyl and aldehyde)

199   displayed weaker or even no fluorescence (Fig. S1a). These differences could be due

200   to the ability of the electron-donating groups to form a larger conjugate system

201   coupled with the benzene ring and decrease the $\pi \rightarrow \pi^*$ transition energy, thus leading

202   to an increase in the Em wavelength (i.e., red shift) and variation in fluorescence

203   intensity (Chen et al., 2002; Andrade-Eiroa et al., 2013). In contrast, the

204   electron-withdrawing group can reduce the conjugated structure formed by the

205   benzene ring and hydroxyl group, reducing the fluorescence intensity

206   (Andrade-Eiroa et al., 2010; Andrade-Eiroa et al., 2013).

207   Aromatic acid and its derivatives are also important light-absorbing organic

208   compounds in atmospheric BrC. Owing to the negative effects of the carboxyl group,

209   a weak fluorescence peak (275/315 nm) was identified for benzoic acid, and no

210   fluorescence was detected for benzene polycarboxylic acids, such as phthalic acid,

211   terephthalic acid, and trimesic acid (Fig. S1b). However, when benzoic acid was

212   substituted with electron-donating groups (e.g., hydroxyl, methoxy), higher intensity

213   fluorescence peaks were observed. Two strong fluorescence peaks at 230/405 and

214   290/405 nm were identified for 2-hydroxybenzoic acid substituted with only one

215   hydroxyl group. These peaks could have been the result of the ortho structure of the

216   hydroxy and carboxyl groups, which is favorable for the formation of intramolecular

hydrogen bonds and generates a double-ring conjugate structure, reducing the

transition energy and thereby presenting strong UV absorption and fluorescence

(Andrade-Eiroa et al., 2013).

N-containing compounds, especially NACs, have strong light absorption, and

have been reported to be the major components of atmospheric BrC, accounting for

more than 60% of the total light absorption intensity at 300–500 nm (Huang et al.,

2021; Lin et al., 2016; Lin et al., 2017; Wang et al., 2017; Frka et al, 2022). However,

most of the NACs did not exhibit any fluorescence (Fig. S1c), similar to that

reported in a previous study by Chen et al. (2020), which could be due to the

significant reduction in the electron density of the benzene ring by the nitro ($-NO_2$)

group—strong electron-withdrawing group—thereby weakening the fluorescence.

Tryptophan and tyrosine are the two most studied PRLIS species, and their

EEM spectra are generally used as standards for comparison with fluorophores in

atmospheric WSOM (Matos et al., 2015; Qin et al., 2018). As shown in Fig. S1d, the

Ex/Em peaks at 275/300 and 275/350 nm corresponded to tyrosine and tryptophan,

respectively. The maximum Em wavelength of phenylalanine was more inclined to

short wavelength (280 nm) and with much weaker fluorescence intensity. Moreover,

the fluorescence peaks of PRLIS obviously overlapped with those of phenols and

aromatic acids (Fig. S1a, b). It must be noted that the concentrations of phenols and

aromatic acids were significantly higher than those of tryptophan and tyrosine in the

atmospheric samples (Table S2); therefore, the aerosol BrC fluorophores in these

regions are more likely to have originated from phenols and aromatic acids rather

239 than PRLIS.

240 N-heterocyclic compounds such as pyrrole, pyridine, and imidazole are

241 commonly identified in atmospheric samples (Dou et al., 2015; Jiang et al., 2019;

242 Kosyakov et al., 2020). However, no fluorescence was observed for these three

243 species in the present study, indicating that the absorbed energy may have been

244 consumed by relaxation or vibration (Fig. S1e). Nevertheless,

245 imidazole-2-formaldehyde produced two strong fluorescence peaks at 290/440 and

246 350/440 nm, formed from the oxidation of imidazole, suggesting that some

247 N-heterocyclic compounds from secondary reactions may exhibit strong

248 fluorescence at higher wavelength in atmospheric BrC (Ackendorf et al., 2017).

249 PAHs and their derivatives are mainly formed from incomplete combustion

250 processes and are important components of BrC (Chen et al., 2020; Lin et al., 2017;

251 Mahamuni et al., 2020). As shown in Fig. S1f, all PAHs exhibited strong

252 fluorescence emission, with its peak location associated with the conjugated

253 aromatic system. Naphthalene presented a fluorescence band located at the

254 maximum Em wavelength of approximately 325 nm. As expected, with the

255 increasing size of the π-bond system and degree of conjugation, the fluorescence

256 band moved toward the longer wavelength range, and a new Em band was observed

257 at 360–390 nm for 3–4-ring phenanthrene and pyrene, and at 400–500 nm for $\geq$

258 5-ring PAHs (Mahamuni et al., 2020). The fluorescence spectra of high-ring PAHs

259 were more complex because of more types of double bonds. As shown in Fig. S1f,

260 the intensity and location of the fluorescence peaks were also significantly changed

when different types of groups were substituted with PAHs. For example, 1-naphthol

exhibited a stronger EEM peak at a relatively longer wavelength (230, 290/460 nm)

owing to its highly conjugated structure, when compared with naphthalene. This

EEM spectrum was located in the EEM region of FAs, implying that FAs are

composed of aromatic units and O-containing groups. In contrast, relatively weaker

fluorescence was observed for 9-fluorenone, anthraquinone, and

2-naphthalenecarboxylic acid, and no EEM signals were observed for

2-nitronaphthol (Fig. S1c), which was substituted with a strong

electron-withdrawing group ($-NO_2$).

3.2. Fluorescence properties of BrC from different sources

As shown in Fig. S4a and S4b, BB and CC WSOM exhibited similar

fluorescence spectra (Tang et al., 2020a; Chen et al., 2020; Yang et al., 2022), with

two types of fluorescence peaks at Ex/Em ≈ (230–240)/(340–400) nm (peak A) and

Ex/Em ≈ (260–280)/(330–360) nm (peak B), respectively. The two fluorescence

peaks were similar to those previously reported for BB WSOM and HULIS (Fan et

al., 2020; Tang et al., 2020a; Yang et al., 2022). In general, peak A mainly

corresponds to the protein-like UV region, with a minor contribution from fulvic-like

substances, whereas peak B could be attributed to tryptophan-like fluorophores.

However, based on the results of the present study, these two peaks could be mainly

attributed to aromatic species such as aromatic acids, phenolic compounds, and

minor quantities of PAHs (e.g., naphthalene) (Fig. 1). The fluorescence spectra of

283 WSOM from two types of vehicles (diesel and gasoline) also presented two

284 fluorophores. A relatively strong fluorescence peak was observed at the low Ex

285 wavelength (Ex/Em $\approx$ 230/350 nm) and a relatively weaker peak was detected at the

286 high Ex wavelength (Ex/Em $\approx$ 270/350 nm) (Fig. S4c). These results are consistent

287 with those reported in previous studies on VE (Chen et al., 2020; Tang et al., 2020a;

288 Yang et al., 2022) and similar to the EEM fluorescence spectra of BB and CC

289 WSOM (Chen et al., 2020; Fan et al., 2020; Cao et al., 2021; Yang et al., 2022).

290 However, the fluorescence ranges of vehicle WSOM were obviously narrower,

291 suggesting that BB and CC WSOM fluorescent components are more complex.

292  Soil-derived DOM is also a primary source of atmospheric WSOM. As shown

293 in Fig. S5a, two main fluorescence peaks located at Ex/Em = 230/430 and 320/430

294 nm, were detected in the fluorescence spectra of soil DOM, which are similar to

295 those reported in previous studies (Ge et al., 2021; Liu et al., 2009) and particularly

296 close to the position of FAs (Fig. S5b).

297  Secondary chemical formation is another important source of atmospheric

298 WSOM. For example, the aqueous-phase reactions of aldehydes with ammonium

299 sulfate (AS) can produce highly fluorescent species (Hawkins et al., 2016). The

300 Glyoxal-AS and glyoxal/glycine reaction products fluoresces at 340/450 nm,

301 whereas formaldehyde-AS reaction product fluoresce at 250/430 nm. Secondary

302 organic aerosols (SOAs) produced in the limonene/O_3 system have been reported to

303 strongly fluoresce in the presence of NH_3 (Bones et al., 2010). In addition, aging of

304 primary organic compounds has also been found to change the fluorescence spectra

305 (Lee et al., 2013; Li et al., 2021; Powelson et al., 2014). For instance, aging of

306 syringic acid with OH radicals caused the initial fluorescence band to move toward

307 the long wavelength range, producing a new band at a broad Em band at 400–600

308 nm. Similarly, the fluorescence peaks red-shifted (e.g., from 260–270/360 nm to

309 280–290/390–400 nm) during the O_3 aging process (Fan et al., 2020), suggesting the

310 degradation of the initial compound and formation of new secondary organic

311 compounds generally located at longer wavelengths, possibly with a high degree of

312 aromaticity or highly oxidized functional groups (Chen et al., 2016a; Vidović et al.,

313 2019, 2020; Powelson et al., 2014; Vione et al., 2019; Yu et al., 2016).

314

315 **3.3. Identification of chemical species and potential sources of fluorescent**

316 **components in ambient aerosols**

317 The typical EEM spectra of atmospheric water-soluble light-absorbing

318 compounds are shown in Fig. 2. Three fluorescence peaks were identified in the

319 aerosol WSOM samples: a stronger fluorescence peak at Ex/Em = 230–250/360–420

320 nm, and two relatively weaker fluorescence peaks at Ex/Em = 270–290/340–370 nm

321 and 300–320/360–420 nm. Similar fluorescence bands have been previously

322 identified in the EEM fluorescence spectra of WSOM from $PM_{2.5}$ in the cold and

323 warm seasons in Aveiro, Portugal (Matos et al., 2015), the High Arctic atmosphere

324 (Fu et al., 2015), Godavari, Nepal (Wu et al., 2019), Lanzhou and Xi'an,

325 northwestern China (Qin et al., 2018; Chen et al., 2020), Chongqing, southwestern

326 China (Wang et al., 2020), and Harbin, northeastern China (Ma et al., 2022).

327 Although the fluorescence intensities varied with different sites and seasons, the

328 shapes of the EEM spectra of WSOM were very similar, making it difficult to

329 directly distinguish the different samples solely based on the characteristics of the

330 EEM profiles. Therefore, a more powerful protocol named the PARAFAC method

331 was employed to identify the individual fluorophores in ambient WSOM.

332

3.3.1. Identification and quantification of fluorescent components by the PARAFAC method

335 As shown in Fig. 3, three fluorescent components (C1, C2, and C3) were

336 identified in the atmospheric samples; C1 occurred at a relatively lower Em

337 wavelength, exhibiting two fluorescence peaks at Ex/Em = 235(270)/330 nm, C2

338 presented fluorescence peaks at around Ex/Em = 235(320)/390 nm, and C3 had a

339 longer Em wavelength than C1 and C2, which was located at Ex/Em = about

340 250(355)/455 nm. In general, these fluorescent components have been interpreted

341 based on knowledge of the fluorescence characteristics of aquatic DOM.

342 Accordingly, C1 is considered to belong to the typical PRLIS (Coble, 1996; Wünsch

343 et al., 2019), C2 is associated with fulvic-like substances or less-oxygenated HULIS

344 (Liu et al., 2009; Zhang et al., 2014), and C3 is usually considered to correspond to

345 terrestrial HULIS that are highly oxygenated organic matter (Table S3) (Liu et al.,

346 2009; Wünsch et al., 2019; Zhou et al., 2017). However, it must be noted that the

347 sources and transformation process are significantly different for WSOM in aerosols

348 and DOM in aquatic and terrestrial environments; therefore, the fluorescence

349 classifications of DOM might not be applicable to atmospheric WSOM.

350 In general, the Ex and Em wavelengths of fluorescent components are mainly

351 associated with their chemical characteristics and structures (Table S1 and Fig. 1). In

352 the present study, C1 was similar to tryptophan-like fluorophores associated with

353 PRLIS in rainwater (Zhang et al., 2014; Zhou et al., 2017) and fog water (Bianco et

354 al., 2014; Bianco et al., 2016). However, this fluorophore might also be related to

355 small molecular aromatic compounds, such as aromatic acids (e.g.,

356 3,5-dihydroxybenzoic acid and 2-naphthalenecarboxylic acid) and PAHs (e.g.,

357 naphthalene, phenanthrene, and anthraquinone) (Fig. 1a) (Miyakawa et al., 2015; Wu

358 et al., 2019). In addition, this fluorophore could also contain traces of some phenolic

359 compounds, including catechol, hydroquinone, and 2-methoxyphenol. These organic

360 species might be generated by various types of combustion processes and

361 atmospheric oxidation reactions. It must be noted that investigations of the

362 fluorescent components in atmospheric WSOM should not only consider their

363 position in the fluorescence spectrum, but also their concentration and possibility of

364 trapping. Many previous studies have reported that the concentration of amino acids

365 in atmospheric aerosols is almost negligible, when compared with that of lower

366 molecular weight aromatic compounds such as aromatic acids and phenolic

367 compounds (Table S2) (Bianco et al., 2016; Song et al., 2017; Vione et al., 2019;

368 Mahamuni et al., 2020; and references therein). Therefore, fluorescent components

369 in this Ex/Em region could be attributed to small molecular aromatic species (e.g,

370 aromatic acids, phenolic compounds) rather than PRLIS. Moreover, this fluorophore

371 overlapped with that of WSOM from combustion process such as BB, CC, and VE

372 (Fig. 1b), suggesting significant contribution of the combustion process.

373   When compared with C1, C2 exhibited a strong fluorescence peak at longer

374 Ex/Em wavelength of 235(320)/390 nm, implying that this fluorescent component

375 presented a relatively larger molecular size and higher aromaticity than C1 (Pöhlker

376 et al., 2012). As shown in Fig. 1a, the fluorescence of C2 is similar to that of

377 aromatic compounds (e.g., 2-naphthalenecarboxylic acid, 2-hydroxybenzoic acid,

378 anthraquinone) and high-ring PAHs (e.g., pyrene, anthraquinone, anthracene,

379 chrysene) (Mahamuni et al., 2020), and overlaps with the fluorescence spectra of

380 FAs. In addition, this fluorophore has also been reported to be related to the

381 generation of SOAs from organic precursors emitted from biological/anthropogenic

382 emission and combustion processes (Wang et al., 2020). For example, the

383 aqueous-phase reactions of aldehydes with AS have been proposed as an important

384 source of atmospheric BrC, which present similar fluorescence spectral profiles

385 (Hawkins et al., 2016; Lee et al., 2013) (Fig. 1b). In addition, oxidative

386 oligomerization of phenols and their derivatives can also shift the Ex/Em wavelength

387 of these substances to longer wavelengths, falling into similar fluorescence regions

388 (Li et al., 2021; Tang et al., 2020a; Vione et al., 2019). As suggested by Chen et al.

389 (2016a), this fluorescent component may be a less-oxygenated fluorescent group

390 contributed by biomass combustion. Therefore, fluorophore C2 might be related to

391 the derivatives of biomass burning and/or biogenic molecules, with relatively lower

392 degree of oxidation (Chen et al., 2016a; Jiang et al., 2022).

393   C3 presented a longer Em wavelength than C1 and C2, with two peaks at

394   around Ex/Em=250/455 nm and 355/455 nm (Fig. 3). This fluorescent component

395   overlaps with the fluorescence of high-ring PAHs and their derivatives, such as

396   fluoranthene, benzo-b-fluoranthene, benzo-a-pyrene, indeno-123cd-pyrene,

397   1-naphthol, and N-heterocyclic compounds, including imidazole-2-formaldehyde

398   (Chen et al., 2020; Mahamuni et al., 2020). Furthermore, this fluorescent component

399   exhibited a similar Ex/Em wavelength to that of FAs and HAs (Fig. S5b), suggesting

400   the possible contribution of soil dust, and thus could be assigned as HULIS (Lin and

401   Guo, 2020). Similar fluorescent substances have also been identified in the study of

402   atmospheric aerosol fluorescent chromophores, such as the highly oxygenated

403   HULIS in Nagoya, Japan (Chen et al., 2016a), Lanzhou, China (Qin et al., 2018),

404   Xi'an, China (Chen et al., 2020), a haze event in Harbin (Ma et al., 2022), and

405   humic-like compounds with more aromatic and unsaturated bonds in Godavari,

406   Nepal (Wu et al., 2019) and Tianjin, China(Deng et al., 2022). Based on the

407   PARAFAC results with aerosol mass spectrometry data, C3 was considered to be a

408   fluorescent group with high oxygen content and high O/C ratio, close to that of aged

409   organic aerosols (Chen et al., 2016a; Jiang et al., 2022) (Fig. 1b). It must be noted

410   that low molecular weight organic compounds can further undergo oligomerization

411   to high molecular weight species with long Em wavelengths during the aging

412   process (Hawkins et al., 2016; Li et al., 2021; Tang et al., 2020b; Yu et al., 2016).

413   The resulting compounds may present a more complex structure than their precursor,

414   probably owing to the presence of condensed aromatic rings and other π-electron

415 systems with a high level of conjugation; thus, atmospheric aging is assumed to be a

416 potential contributor to C3 (Barsotti et al., 2016; De Laurentiis et al., 2013; Hawkins

417 et al., 2016).

418

419 **3.3.2. Spatial and seasonal variations in fluorescent components in WSOM**

420   The relative contributions of C1, C2, and C3 components to the total

421 fluorescence intensities ($F_{max}/\sum F_{max}$) were calculated (Fig. 4), and were found to be

422 similar for WSOM from CZ and GZ, exhibiting maximum C2 content and relatively

423 lower C1 and C3 contents. Furthermore, WSOM samples showed obvious spatial

424 and seasonal variations, similar to the results reported in other regions in China

425 (Zhang et al., 2022a, 2022b). First, CZ WSOM presented a relatively higher C3

426 content (23±4%) than GZ WSOM (17±3%), whereas GZ WSOM had a relatively

427 higher C2 content (56±7%) than CZ WSOM (49±4%) during the same sampling

428 period. Such differences in the composition of fluorescent components may be

429 ascribed to the variation in the primary emission sources and atmospheric aging

430 process at the two sites. The relatively higher C3 content in the CZ could be

431 attributed to the comparatively high contribution of soil dust in the suburban region,

432 which is consistent with the relatively higher Ca^{2+} contents in the CZ $PM_{2.5}$

433 (1.8±1.2%) than in the GZ $PM_{2.5}$ (1.5±0.8%) (Vasilatou et al., 2017; Wu et al., 2019).

434 In contrast, the relatively higher C2 content in GZ WSOM may be attributed to the

435 comparatively stronger atmospheric chemical reaction associated with bio-volatile

436 organic compounds (bio-VOCs) in the hot and humid region of GZ. This result was

consistent with the relatively higher humification index (HIX) and normalized

fluorescence volume (NFV) values (log(NFV)) of CZ WSOM (Fig. S6) (Chen et al.,

2020; Yang et al., 2022).

In addition, the resolved Ex and Em spectra for GZ WSOM were also similar in

different seasons, implying that the types of fluorophores contributing to WSOM

were predominantly the same throughout the year. However, the compositions of

fluorescent components varied in different seasons. In the dry season (October–

March), WSOM showed relatively higher contents of C3 fluorophores (17±4%),

whereas in the wet season (April–September), slightly higher contents of C2

fluorophores (69±4%) were detected (Fig. 4) (Chen et al., 2020; Wang et al., 2020).

These differences might be associated with the variations in the source composition

and aging effects of BrC in different seasons. The higher content of C3 in WSOM in

the dry season suggested the occurrence of more highly aromatic and highly

oxidized compounds. These results could be explained by the fact that more aged

organic aerosols and dust were transported from the northern region of China (Jiang

et al., 2021). In contrast, the slightly higher C2 content in the wet season may be

attributed to the relatively stronger secondary formation of bio-SOAs and

photodegradation effects in the high-temperature and relative humidity season.

4. Conclusion and future prospects

In this study, the fluorescence properties of BrC model compounds were

investigated to determine the chromophoric species that can be evaluated by the

459   EEM method. Accordingly, the aerosol WSOM samples at two sites (CZ and GZ)

460   were investigated by the EEM-PARAFAC method, and the chemical characteristics

461   and potential sources of fluorescent components were examined. The main

462   conclusions and future prospects are as follows:

463   (1) Fluorescent components have predominantly been evaluated based on the

464   knowledge of fluorophores in aquatic DOM, which often leads to misinterpretation.

465   In the present study, the chemical characteristics of fluorophores in different Ex/Em

466   regions were discussed based on the fluorescence properties of BrC model

467   compounds and their amounts in aerosols. In particular, the C1 fluorophore in

468   atmospheric WSOM, which has been frequently assigned to PRLIS because of the

469   similarity in fluorescence spectra, was demonstrated to mainly include aromatic

470   acids, phenolic compounds, and their derivatives, with negligible amounts of amino

471   acids.

472   (2) The fluorescence properties of target compounds are mainly influenced by

473   the aromatic system and characteristics of adjacent functional groups. Organic

474   compounds with high aromaticity and strong electron-donating groups (e.g.,

475   hydroxyl, methoxyl) generally exhibited strong fluorescence spectra at longer Em

476   wavelengths, whereas organic compounds substituted with electron-withdrawing

477   groups presented relatively weaker fluorescence intensities. In particular, aromatic

478   compounds containing nitro groups (i.e., nitrophenols) showed strong absorption and

479   were the major component of atmospheric BrC; however, they did not exhibit

480   significant fluorescene. Thus, the fluorescence method could only measure a subset

of chromophores in aerosol BrC and should be used with caution for the investigation of aerosol BrC.

(3) The EEM spectra for aerosol WSOM were very similar; however, the relative contents of certain fluorescent components significantly varied with the sampling site and season. For example, more fluorescent components associated with soil and secondary oxidation of small molecular compounds from combustion emission were identified in CZ WSOM, whereas more fluorescent components derived from atmospheric chemical reaction of bio-VOCs were observed in GZ WSOM. In addition, GZ WSOM exhibited more highly aromatic and highly oxidized compounds in the dry season.

Although many studies have applied the EEM-PARAFAC method to investigate atmospheric WSOM and have obtained useful data, there are still challenges and gaps that must be addressed. First, caution should be taken for credible interpretations of the fluorescent components in atmospheric WSOM because of the differences in chemical characteristics of organic matter derived from different sources. In addition, the same fluorophores may exhibit different Ex/Em ranges and intensities in different environmental conditions (e.g., pH, coexisting metal ions and inorganic salts). Therefore, more theoretical and experimental studies are necessary to understand the relationship between the fluorescent groups and positions of fluorescence peaks, as well as the influences of sources and chemical formation process of the fluorescent groups on fluorescence peaks.

Data availability

The research data can be accessed in the Harvard Dataverse (https://doi.org/10.7910/DVN/ULCIU9, Song, 2022)

Author contributions. J. Song designed the research. T. Cao and C. Xu, analyzed the model compounds and WSOM samples by UV-Vis and EEM. T. Cao and X. Fan resolved the EEM by PARAFAC tool. M. Li carried out the $PM_{2.5}$ sampling experiments. T. Cao and J. Song wrote the paper. J. Li, W. Jia, and P. Peng commented and revised the paper.

Competing interests. The authors declare that they have no conflict of interest

Acknowledgments. The present work was supported by the National Natural Science Foundation of China (42192514 and 41977188), Guangdong Foundation for Program of Science and Technology Research (2020B1212060053), and Guangdong Foundation for Program of Science and Technology Research (2019B121205006).

References

Ackendorf, J. M., Ippolito, M. G., and Galloway, M. M.: pH Dependence of the Imidazole-2-carboxaldehyde Hydration Equilibrium: Implications for Atmospheric Light Absorbance, Environ. Sci. Tech. Let., 4, 551-555, http://doi.org/10.1021/acs.estlett.7b00486, 2017.

525 Aftab, B., Shin, H. S., and Hur, J.: Exploring the fate and oxidation behaviors of

526   different organic constituents in landfill leachate upon Fenton oxidation

527   processes using EEM-PARAFAC and 2D-COS-FTIR, J. Haza. Mat., 354, 33-41,

528   http://doi.org/10.1016/j.jhazmat.2018.04.059, 2018.

529 Andrade-Eiroa, A., Leroy, V., and Dagaut, P.: Advances in PAHs/nitro-PAHs

530   fractioning, Anal. Meth., 2, 2017, http://doi.org/10.1039/c0ay00484g, 2010.

531 Andrade-Eiroa, Á., Canle, M., and Cerdá, V.: Environmental Applications of

532   Excitation-Emission Spectrofluorimetry: An In-Depth Review I, Appl. Spec.

533   Rev., 48, 1-49, http://doi.org/10.1080/05704928.2012.692104, 2013.

534 Barsotti, F., Ghigo, G., and Vione, D.: Computational assessment of the fluorescence

535   emission of phenol oligomers: A possible insight into the fluorescence

536   properties of humic-like substances (HULIS), J. Photo. Photo. A., 315, 87-93,

537   http://doi.org/10.1016/j.jphotochem.2015.09.012, 2016.

538 Bianco, A., Minella, M., De Laurentiis, E., Maurino, V., Minero, C., and Vione, D.:

539   Photochemical generation of photoactive compounds with fulvic-like and

540   humic-like fluorescence in aqueous solution, Chemosphere, 111, 529-536,

541   http://doi.org/10.1016/j.chemosphere.2014.04.035, 2014.

542 Bianco, A., Passananti, M., Deguillaume, L., Mailhot, G., and Brigante, M.:

543   Tryptophan and tryptophan-like substances in cloud water: Occurrence and

544   photochemical fate, Atmos. Environ., 137, 53-61,

545   http://doi.org/10.1016/j.atmosenv.2016.04.034, 2016.

546   Bones, D. L., Henricksen, D. K., Mang, S. A., Gonsior, M., Bateman, A. P., Nguyen,

547   T. B., Cooper, W. J., and Nizkorodov, S. A.: Appearance of strong absorbers and

548   fluorophores in limonene-O_3 secondary organic aerosol due to NH4$^+$-mediated

549   chemical aging over long time scales, J Geophys Res-Atmos, 115, D05203,

550   http://doi.org/10.1029/2009jd012864, 2010.

551   Cao, T., Li, M. J., Zou, C. L., Fan, X. J., Song, J. Z., Jia, W. L., Yu, C. L., Yu, Z. Q.,

552   and Ping, P. A.: Chemical composition, optical properties, and oxidative

553   potential of water- and methanol-soluble organic compounds emitted from the

554   combustion of biomass materials and coal, Atmos. Chem. Phys., 21,

555   13187-13205, http://doi.org/10.5194/acp-21-13187-2021, 2021.

556   Chen, J., Gu, B. H., LeBoeuf, E. J., Pan, H. J., and Dai, S.: Spectroscopic

557   characterization of the structural and functional properties of natural organic

558   matter fractions, Chemosphere, 48, 59-68,

559   https://doi.org/10.1016/s0045-6535(02)00041-3, 2002.

560   Chen, Q., Ikemori, F., and Mochida, M.: Light Absorption and Excitation-Emission

561   Fluorescence of Urban Organic Aerosol Components and Their Relationship to

562   Chemical Structure, Environ. Sci. Tech., 50, 10859-10868,

563   http://doi.org/10.1021/acs.est.6b02541, 2016a.

564   Chen, Q., Miyazaki, Y., Kawamura, K., Matsumoto, K., Coburn, S., Volkamer, R.,

565   Iwamoto, Y., Kagami, S., Deng, Y., Ogawa, S., Ramasamy, S., Kato, S., Ida, A.,

566   Kajii, Y., and Mochida, M.: Characterization of Chromophoric Water-Soluble

567   Organic Matter in Urban, Forest, and Marine Aerosols by HR-ToF-AMS

568   Analysis and Excitation-Emission Matrix Spectroscopy, Environ. Sci. Tech., 50,

569   10351-10360, http://doi.org/10.1021/acs.est.6b01643, 2016b.

570 Chen, Q., Li, J., Hua, X., Jiang, X., Mu, Z., Wang, M., Wang, J., Shan, M., Yang, X.,

571   Fan, X., Song, J., Wang, Y., Guan, D., and Du, L.: Identification of species and

572   sources of atmospheric chromophores by fluorescence excitation-emission

573   matrix with parallel factor analysis, Sci. Total Environ., 718, 137322,

574   http://doi.org/10.1016/j.scitotenv.2020.137322, 2020.

575 Coble, P. G.: Characterization of marine and terrestrial DOM in seawater using

576   excitation emission matrix spectroscopy, Marin. Chem., 51, 325-346,

577   http://doi.org/10.1016/0304-4203(95)00062-3, 1996.

578 Coble, P. G.: Marine optical biogeochemistry: The chemistry of ocean color, Chem.

579   Rev., 107, 402-418, http://doi.org/10.1021/cr050350+, 2007.

580 De Laurentiis, E., Maurino, V., Minero, C., Vione, D., Mailhot, G., and Brigante, M.:

581   Could triplet-sensitised transformation of phenolic compounds represent a

582   source of fulvic-like substances in natural waters?, Chemosphere, 90, 881-884,

583   http://doi.org/10.1016/j.chemosphere.2012.09.031, 2013.

584 Deng, J., Ma, H., Wang, X., Zhong, S., Zhang, Z., Zhu, J., Fan, Y., Hu, W., Wu, L.,

585   Li, X., Ren, L., Pavuluri, C. M., Pan, X., Sun, Y., Wang, Z., Kawamura, K., and

586   Fu, P.: Measurement report: Optical properties and sources of water-soluble

587   brown carbon in Tianjin, North China – insights from organic molecular

588   compositions, Atmos. Chem. Phys., 22, 6449-6470,

589   https://doi.org/10.5194/acp-22-6449-2022, 2022.

Dou, J., Lin, P., Kuang, B. Y., and Yu, J. Z.: Reactive Oxygen Species Production Mediated by Humic-like Substances in Atmospheric Aerosols: Enhancement Effects by Pyridine, Imidazole, and Their Derivatives, Environ. Sci. Tech., 49, 6457-6465, http://doi.org/10.1021/es5059378, 2015.

Fan, X., Cao, T., Yu, X., Wang, Y., Xiao, X., Li, F., Xie, Y., Ji, W., Song, J., Peng, P., amp, apos, and an: The evolutionary behavior of chromophoric brown carbon during ozone aging of fine particles from biomass burning, Atmos. Chem. Phys., 20, 4593-4605, http://doi.org/10.5194/acp-20-4593-2020, 2020.

Frka, S., Šala, M., Brodnik, H., Štefane, B., Kroflič, A., and Grgić, I.: Seasonal variability of nitroaromatic compounds in ambient aerosols: Mass size distribution, possible sources and contribution to water-soluble brown carbon light absorption, Chemosphere, 299, 134381, https://doi.org/10.1016/j.chemosphere.2022.134381, 2022.

Fu, P., Kawamura, K., Chen, J., Qin, M., Ren, L., Sun, Y., Wang, Z., Barrie, L. A., Tachibana, E., Ding, A., and Yamashita, Y.: Fluorescent water-soluble organic aerosols in the High Arctic atmosphere, Sci. Rep., 5, 9845, http://doi.org/10.1038/srep09845, 2015.

Ge, Z., Gao, L., Ma, N., Hu, E., and Li, M.: Variation in the content and fluorescent composition of dissolved organic matter in soil water during rainfall-induced wetting and extract of dried soil, Sci. Total Environ., 791, 148296, http://doi.org/10.1016/j.scitotenv.2021.148296, 2021.

Graber, E. R., and Rudich, Y.: Atmospheric HULIS: How humic-like are they? A comprehensive and critical review, Atmos. Chem. Phys., 6, 729-753, http://doi.org/10.5194/acp-6-729-2006, 2006.

Hawkins, L. N., Lemire, A. N., Galloway, M. M., Corrigan, A. L., Turley, J. J., Espelien, B. M., and De Haan, D. O.: Maillard Chemistry in Clouds and Aqueous Aerosol As a Source of Atmospheric Humic-Like Substances, Environ. Sci. Tech., 50, 7443-7452, http://doi.org/10.1021/acs.est.6b00909, 2016.

Huang, R.-J., Yang, L., Shen, J., Yuan, W., Gong, Y., Ni, H., Duan, J., Yan, J., Huang, H., You, Q., and Li, Y. J.: Chromophoric Fingerprinting of Brown Carbon from Residential Biomass Burning, Environ. Sci. Tech. Let., 9, 102-111, http://doi.org/10.1021/acs.estlett.1c00837, 2021.

Huang, S., Luo, Y., Wang, X., Zhang, T., Lei, Y., Zeng, Y., Sun, J., Che, H., Xu, H., Cao, J., and Shen, Z.: Optical properties, chemical functional group, and oxidative activity of different polarity levels of water-soluble organic matter in PM2.5 from biomass and coal combustion in rural areas in Northwest China, Atmos. Environ., 283, 119179, https://doi.org/10.1016/j.atmosenv.2022.119179, 2022.

Huo, Y. Q., Li, M., Jiang, M. H., and Qi, W. M.: Light absorption properties of HULIS in primary particulate matter produced by crop straw combustion under different moisture contents and stacking modes, Atmos. Environ., 191, 490-499, http://doi.org/10.1016/j.atmosenv.2018.08.038, 2018.

Jiang, H., Frie, A. L., Lavi, A., Chen, J. Y., Zhang, H., Bahreini, R., and Lin, Y.-H.: Brown Carbon Formation from Nighttime Chemistry of Unsaturated Heterocyclic Volatile Organic Compounds, Environ. Sci. Tech. Let., 6, 184-190, http://doi.org/10.1021/acs.estlett.9b00017, 2019.

Jiang, H., Tang, J., Li, J., Zhao, S., Mo, Y., Tian, C., Zhang, X., Jiang, B., Liao, Y., Song, J., Chen, Y., Zhang, G., 2022. Molecular Signatures of Fluorescence Components in Atmospheric Organic Matters Inferred from Positive and Negative Electrospray Ionization Fourier Transform Ion Cyclotron Resonance Mass Spectrometry. Environ. Sci. Tech. Let., 9, 11, 913-920., https://doi.org/10.1021/acs.estlett.2c00629, 2022.

Jiang, H. X., Li, J., Sun, R., Liu, G. Q., Tian, C. G., Tang, J., Cheng, Z. N., Zhu, S. Y., Zhong, G. C., Ding, X., and Zhang, G.: Determining the Sources and Transport of Brown Carbon Using Radionuclide Tracers and Modeling, J Geophys Res-Atmos, 126, e2021JD034616, http://doi.org/10.1029/2021JD034616, 2021.

Kosyakov, D. S., Ul'yanovskii, N. V., Latkin, T. B., Pokryshkin, S. A., Berzhonskis, V. R., Polyakova, O. V., and Lebedev, A. T.: Peat burning – An important source of pyridines in the earth atmosphere, Environ. Pollut., 266, 115109, http://doi.org/10.1016/j.envpol.2020.115109, 2020.

Laskin, A., Laskin, J., and Nizkorodov, S. A.: Chemistry of atmospheric brown carbon, Chem. Rev., 115, 4335-4382, http://doi.org/10.1021/cr5006167, 2015.

Lee, H. J., Laskin, A., Laskin, J., and Nizkorodov, S. A.: Excitation-emission spectra and fluorescence quantum yields for fresh and aged biogenic secondary organic

aerosols, Environ. Sci. Tech., 47, 5763-5770, http://doi.org/10.1021/es400644c, 2013.

Li, F., Tsona, N. T., Li, J., and Du, L.: Aqueous-phase oxidation of syringic acid emitted from biomass burning: Formation of light-absorbing compounds, Sci. Total Environ., 765, 144239, http://doi.org/10.1016/j.scitotenv.2020.144239, 2021.

Lin, H., and Guo, L.: Variations in Colloidal DOM Composition with Molecular Weight within Individual Water Samples as Characterized by Flow Field-Flow Fractionation and EEM-PARAFAC Analysis, Environ. Sci. Tech., 54, 1657-1667, http://doi.org/10.1021/acs.est.9b07123, 2020.

Lin, P., Aiona, P. K., Li, Y., Shiraiwa, M., Laskin, J., Nizkorodov, S. A., and Laskin, A.: Molecular Characterization of Brown Carbon in Biomass Burning Aerosol Particles, Environ. Sci. Tech., 50, 11815-11824, http://doi.org/10.1021/acs.est.6b03024, 2016.

Lin, P., Bluvshtein, N., Rudich, Y., Nizkorodov, S. A., Laskin, J., and Laskin, A.: Molecular Chemistry of Atmospheric Brown Carbon Inferred from a Nationwide Biomass Burning Event, Environ. Sci. Tech., 51, 11561-11570, http://doi.org/10.1021/acs.est.7b02276, 2017.

Liu, L., Song, C., Yan, Z., and Li, F.: Characterizing the release of different composition of dissolved organic matter in soil under acid rain leaching using three-dimensional excitation-emission matrix spectroscopy, Chemosphere, 77, 15-21, http://doi.org/10.1016/j.chemosphere.2009.06.026, 2009.

Ma, L., Li, B., Yabo, S. D., Li, Z., and Qi, H.: Fluorescence fingerprinting characteristics of water-soluble organic carbon from size-resolved particles during pollution event, Chemosphere, 307, 135748, https://doi.org/10.1016/j.chemosphere.2022.135748, 2022.

Mahamuni, G., Rutherford, J., Davis, J., Molnar, E., Posner, J. D., Seto, E., Korshin, G., and Novosselov, I.: Excitation–Emission Matrix Spectroscopy for Analysis of Chemical Composition of Combustion Generated Particulate Matter, Environ. Sci. Tech., 54, 8198-8209, http://doi.org/10.1021/acs.est.0c01110, 2020.

Matos, J. T. V., Freire, S. M. S. C., Duarte, R. M. B. O., and Duarte, A. C.: Natural organic matter in urban aerosols: Comparison between water and alkaline soluble components using excitation-emission matrix fluorescence spectroscopy and multiway data analysis, Atmos. Environ., 102, 1-10, http://doi.org/10.1016/j.atmosenv.2014.11.042, 2015.

Miyakawa, T., Kanaya, Y., Taketani, F., Tabaru, M., Sugimoto, N., Ozawa, Y., and Takegawa, N.: Ground-based measurement of fluorescent aerosol particles in Tokyo in the spring of 2013: Potential impacts of nonbiological materials on autofluorescence measurements of airborne particles, J Geophys Res-Atmos., 120, 1171-1185, http://doi.org/10.1002/2014jd022189, 2015.

Murphy, K. R., Butler, K. D., Spencer, R. G. M., Stedmon, C. A., Boehme, J. R., and Aiken, G. R.: Measurement of Dissolved Organic Matter Fluorescence in Aquatic Environments: An Interlaboratory Comparison, Environ. Sci. Tech., 44, 9405-9412, http://doi.org/10.1021/es102362t, 2010.

698   Murphy, K. R., Stedmon, C. A., Graeber, D., and Bro, R.: Fluorescence spectroscopy

699   and multi-way techniques. PARAFAC, Anal. Meth., 5, 6557,

700   http://doi.org/10.1039/c3ay41160e, 2013.

701   Murphy, K. R., Timko, S. A., Gonsior, M., Powers, L. C., Wünsch, U. J., and

702   Stedmon, C. A.: Photochemistry Illuminates Ubiquitous Organic Matter

703   Fluorescence Spectra, Environ. Sci. Tech., 52, 11243-11250,

704   http://doi.org/10.1021/acs.est.8b02648, 2018.

705   Niu, X., Pu, W., Fu, P., Chen, Y., Xing, Y., Wu, D., Chen, Z., Shi, T., Zhou, Y., Wen,

706   H., and Wang, X.: Fluorescence characteristics, absorption properties, and

707   radiative effects of water-soluble organic carbon in seasonal snow across

708   northeastern China, Atmos. Chem. Phys., 22, 14075-14094,

709   https://doi.org/10.5194/acp-22-14075-2022, 2022.

710   Pöhlker, C., Huffman, J. A., and Pöschl, U.: Autofluorescence of atmospheric

711   bioaerosols – fluorescent biomolecules and potential interferences, Atmos.

712   Meas. Tech., 5, 37-71, http://doi.org/10.5194/amt-5-37-2012, 2012.

713   Powelson, M. H., Espelien, B. M., Hawkins, L. N., Galloway, M. M., and De Haan,

714   D. O.: Brown carbon formation by aqueous-phase carbonyl compound reactions

715   with amines and ammonium sulfate, Environ. Sci. Tech., 48, 985-993,

716   http://doi.org/10.1021/es4038325, 2014.

717   Qin, J., Zhang, L., Zhou, X., Duan, J., Mu, S., Xiao, K., Hu, J., and Tan, J.:

718   Fluorescence fingerprinting properties for exploring water-soluble organic

compounds in PM$_{2.5}$ in an industrial city of northwest China, Atmos. Environ.,
184, 203-211, http://doi.org/10.1016/j.atmosenv.2018.04.049, 2018.

Smith, J. D., Kinney, H., and Anastasio, C.: Phenolic carbonyls undergo rapid
aqueous photodegradation to form low-volatility, light-absorbing products,
Atmos. Environ., 126, 36-44, http://doi.org/10.1016/j.atmosenv.2015.11.035,
2016.

Song, J.: Data for CT, Harvard Dataverse [data set], (https://
doi.org/10.7910/DVN/ULCIU9, 2022.

Song, T., Wang, S., Zhang, Y., Song, J., Liu, F., Fu, P., Shiraiwa, M., Xie, Z., Yue, D.,
Zhong, L., Zheng, J., and Lai, S.: Proteins and Amino Acids in Fine Particulate
Matter in Rural Guangzhou, Southern China: Seasonal Cycles, Sources, and
Atmospheric Processes, Environ. Sci. Tech., 51, 6773-6781,
https://doi.org/10.1021/acs.est.7b00987, 2017.

Tang, J., Li, J., Su, T., Han, Y., Mo, Y., Jiang, H., Cui, M., Jiang, B., Chen, Y., Tang,
J., Song, J., Peng, P. a., and Zhang, G.: M.olecular compositions and optical
properties of dissolved brown carbon in biomass burning, coal combustion, and
vehicle emission aerosols illuminated by excitation–emission matrix
spectroscopy and Fourier transform ion cyclotron resonance mass spectrometry
analysis, Atmos. Chem. Phys., 20, 2513-2532,
http://doi.org/10.5194/acp-20-2513-2020, 2020a.

Tang, J., Wang, J., Zhong, G., Jiang, H., Mo, Y., Zhang, B., Geng, X., Chen, Y., Tang,
J., Tian, C., Bualert, S., Li, J., and Zhang, G.: Measurement report:

Long-emission-wavelength chromophores dominate the light absorption of brown carbon in aerosols over Bangkok: impact from biomass burning, Atmos. Chem. Phys., 21, 11337-11352, http://doi.org/10.5194/acp-21-11337-2021, 2021.

Tang, S., Li, F., Tsona, N. T., Lu, C., Wang, X., and Du, L.: Aqueous-Phase Photooxidation of Vanillic Acid: A Potential Source of Humic-Like Substances (HULIS), ACS Ear. Spac. Chem, 4, 862-872, http://doi.org/10.1021/acsearthspacechem.0c00070, 2020b.

Vasilatou, V., Diapouli, E., Abatzoglou, D., Bakeas, E. B., Scoullos, M., and Eleftheriadis, K.: Characterization of $PM_{2.5}$ chemical composition at the Demokritos suburban station, in Athens Greece. The influence of Saharan dust, Environ. Sci. Pollut. Res., 24, 11836-11846, https://doi.org/10.1007/s11356-017-8684-3, 2017.

Vidović, K., Kroflič, A., Jovanovič, P., Šala, M., and Grgić, I.: Electrochemistry as a Tool for Studies of Complex Reaction Mechanisms: The Case of the Atmospheric Aqueous-Phase Aging of Catechols, Environ. Sci. Tech., 53, 11195-11203, https://doi.org/10.1021/acs.est.9b02456, 2019.

Vidović, K., Kroflič, A., Šala, M., and Grgić, I.: Aqueous-Phase Brown Carbon Formation from Aromatic Precursors under Sunlight Conditions, Atmosphere, 11, 131, https://doi.org/10.3390/atmos11020131, 2020.

Vione, D., Albinet, A., Barsotti, F., Mekic, M., Jiang, B., Minero, C., Brigante, M., and Gligorovski, S.: Formation of substances with humic-like fluorescence

properties, upon photoinduced oligomerization of typical phenolic compounds emitted by biomass burning, Atmos. Environ., 206, 197-207, http://doi.org/10.1016/j.atmosenv.2019.03.005, 2019.

Wünsch, U. J., Bro, R., Stedmon, C. A., Wenig, P., and Murphy, K. R.: Emerging patterns in the global distribution of dissolved organic matter fluorescence, Anal. Meth., 11, 888-893, http://doi.org/10.1039/c8ay02422g, 2019.

Wang, H., Zhang, L., Huo, T., Wang, B., Yang, F., Chen, Y., Tian, M., Qiao, B., and Peng, C.: Application of parallel factor analysis model to decompose excitation-emission matrix fluorescence spectra for characterizing sources of water-soluble brown carbon in $PM_{2.5}$, Atmos. Environ., 223, 117192, http://doi.org/10.1016/j.atmosenv.2019.117192, 2020.

Wozniak, A. S., Bauer, J. E., and Dickhut, R. M.: Characteristics of water-soluble organic carbon associated with aerosol particles in the eastern United States, Atmos. Environ., 46, 181-188, https://doi.org/10.1016/j.atmosenv.2011.10.001, 2012.

Wu, G., Ram, K., Fu, P., Wang, W., Zhang, Y., Liu, X., Stone, E. A., Pradhan, B. B., Dangol, P. M., Panday, A. K., Wan, X., Bai, Z., Kang, S., Zhang, Q., and Cong, Z.: Water-Soluble Brown Carbon in Atmospheric Aerosols from Godavari (Nepal), a Regional Representative of South Asia, Environ. Sci. Tech., 53, 3471-3479, http://doi.org/10.1021/acs.est.9b00596, 2019.

Wu, G., Fu, P., Ram, K., Song, J., Chen, Q., Kawamura, K., Wan, X., Kang, S., Wang, X., Laskin, A., and Cong, Z.: Fluorescence characteristics of

water-soluble organic carbon in atmospheric aerosol, Environ. Pollut., 268, 115906, http://doi.org/10.1016/j.envpol.2020.115906, 2020.

Wu, L., Luo, X.-S., Li, H., Cang, L., Yang, J., Yang, J., Zhao, Z., and Tang, M.: Seasonal Levels, Sources, and Health Risks of Heavy Metals in Atmospheric $PM_{2.5}$ from Four Functional Areas of Nanjing City, Eastern China, Atmosphere, 10, 419, https://doi.org/10.3390/atmos10070419, 2019.

Yan, G., and Kim, G.: Speciation and Sources of Brown Carbon in Precipitation at Seoul, Korea: Insights from Excitation-Emission Matrix Spectroscopy and Carbon Isotopic Analysis, Environ. Sci. Tech., 51, 11580-11587, http://doi.org/10.1021/acs.est.7b02892, 2017.

Yang, Y., Qin, Y., Qin, J., Zhou, X., Xv, P., Tan, J., and Xiao, K.: Facile Differentiation of Four Sources of Water-Soluble Organic Carbon in Atmospheric Particulates Using Multiple Fluorescence Spectral Fingerprints, Environ. Sci. Tech. Let., 9, 359-365, http://doi.org/10.1021/acs.estlett.2c00128, 2022.

Yu, L., Smith, J., Laskin, A., Anastasio, C., Laskin, J., and Zhang, Q.: Chemical characterization of SOA formed from aqueous-phase reactions of phenols with the triplet excited state of carbonyl and hydroxyl radical, Atmos. Chem. Phys., 14, 13801-13816, http://doi.org/10.5194/acp-14-13801-2014, 2014.

Yu, L., Smith, J., Laskin, A., George, K. M., Anastasio, C., Laskin, J., Dillner, A. M., and Zhang, Q.: Molecular transformations of phenolic SOA during photochemical aging in the aqueous phase: competition among oligomerization,

807   functionalization, and fragmentation, Atmos. Chem. Phys., 16, 4511-4527,

808   http://doi.org/10.5194/acp-16-4511-2016, 2016.

809   Zhang, T., Shen, Z. X., Zeng, Y. L., Cheng, C. L., Wang, D. W., Zhang, Q., Lei, Y. L.,

810   Zhang, Y., Sun, J., Xu, H. M., Ho, S. S. H., and Cao, J. J.: Light absorption

811   properties and molecular profiles of HULIS in $PM_{2.5}$ emitted from biomass

812   burning in traditional "Heated Kang" in Northwest China, Sci. Total Environ.,

813   776, https://doi.org/10.1016/j.scitotenv.2021.146014, 2021.

814   Zhang, T., Shen, Z., Huang, S., Lei, Y., Zeng, Y., Sun, J., Zhang, Q., Ho, S. S. H., Xu,

815   H., and Cao, J.: Optical properties, molecular characterizations, and oxidative

816   potentials of different polarity levels of water-soluble organic matters in winter

817     $PM_{2.5}$ in six China's megacities, Sci. Total Environ., 853, 158600,

818   https://doi.org/10.1016/j.scitotenv.2022.158600, 2022a.

819   Zhang, T., Huang, S., Wang, D., Sun, J., Zhang, Q., Xu, H., Hang Ho, S. S., Cao, J.,

820   and Shen, Z.: Seasonal and diurnal variation of $PM_{2.5}$ HULIS over Xi'an in

821   Northwest China: Optical properties, chemical functional group, and

822   relationship with reactive oxygen species (ROS), Atmos. Environ., 268, 118782,

823   https://doi.org/10.1016/j.atmosenv.2021.118782, 2022b.

824   Zhang, X. L., Lin, Y. H., Surratt, J. D., and Weber, R. J.: Sources, Composition and

825   Absorption Angstrom Exponent of Light-absorbing Organic Components in

826   Aerosol Extracts from the Los Angeles Basin, Environ. Sci. Tech., 47,

827   3685-3693, http://doi.org/10.1021/es305047b, 2013.

828 Zhang, Y. L., Gao, G., Shi, K., Niu, C., Zhou, Y. Q., Qin, B. Q., and Liu, X. H.:

829   Absorption and fluorescence characteristics of rainwater CDOM and

830   contribution to Lake Taihu, China, Atmos. Environ., 98, 483-491,

831   http://doi.org/10.1016/j.atmosenv.2014.09.038, 2014.

832 Zhao, W. Y., Fu, P. Q., Yue, S. Y., Li, L. J., Xie, Q. R., Zhu, C., Wei, L. F., Ren, H.,

833   Li, P., Li, W. J., Sun, Y. L., Wang, Z. F., Kawamura, K., and Chen, J. M.:

834   Excitation-emission matrix fluorescence, molecular characterization and

835   compound-specific stable carbon isotopic composition of dissolved organic

836   matter in cloud water over Mt. Tai, Atmos. Environ., 213, 608-619,

837   http://doi.org/10.1016/j.atmosenv.2019.06.034, 2019.

838 Zheng, G., He, K., Duan, F., Cheng, Y., and Ma, Y.: Measurement of humic-like

839   substances in aerosols: a review, Environ. Pollut., 181, 301-314,

840   http://doi.org/10.1016/j.envpol.2013.05.055, 2013.

841 Zhou, Y., West, C. P., Hettiyadura, A. P. S., Niu, X., Wen, H., Cui, J., Shi, T., Pu, W.,

842   Wang, X., and Laskin, A.: Measurement report: Molecular composition, optical

843   properties, and radiative effects of water-soluble organic carbon in snowpack

844   samples from northern Xinjiang, China, Atmos. Chem. Phys., 21, 8531-8555,

845   https://doi.org/10.5194/acp-21-8531-2021, 2021.

846 Zhou, Y., Yao, X., Zhang, Y., Shi, K., Zhang, Y., Jeppesen, E., Gao, G., Zhu, G., and

847   Qin, B.: Potential rainfall-intensity and pH-driven shifts in the apparent

848   fluorescent composition of dissolved organic matter in rainwater, Environ.

849   Pollut., 224, 638-648, http://doi.org/10.1016/j.envpol.2017.02.048, 2017.

(a)
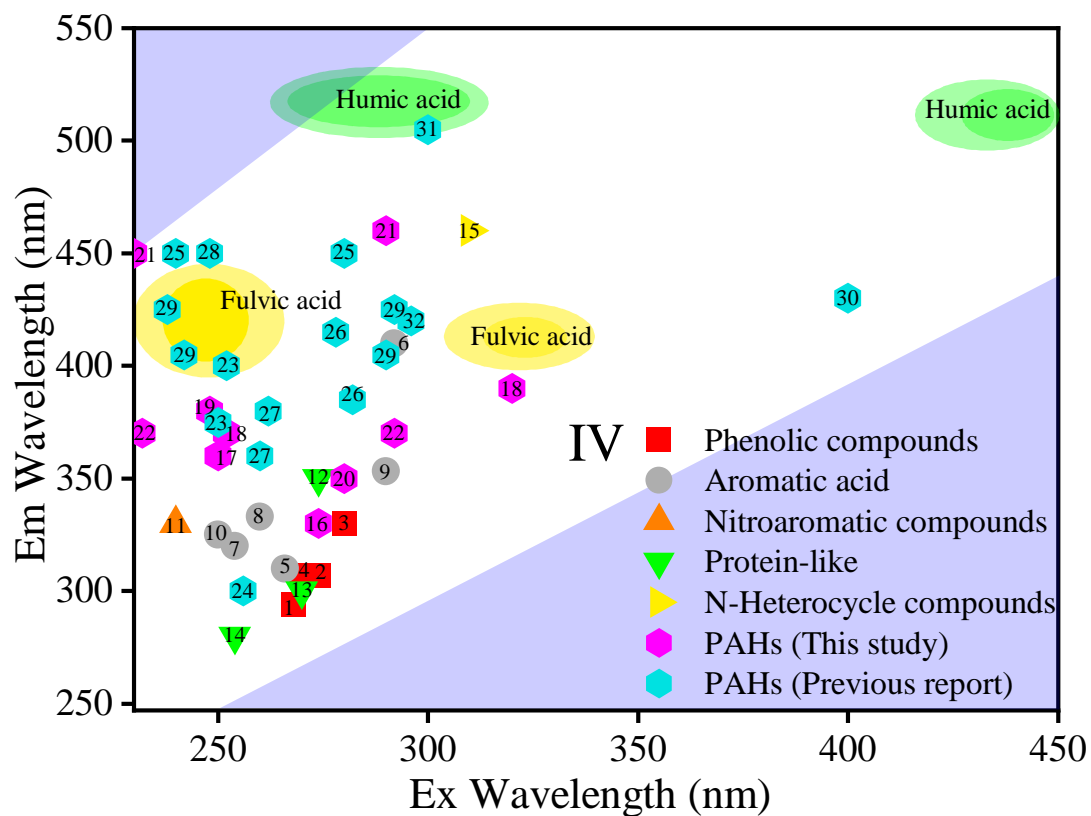
1: Phenol	2: Catechol	3: Hydroquinone
4: 2-Methoxyphenol	5: Benzoic acid	6: 2-Hydroxybenzoic acid
7: 4-Hydroxybenzoic acid	8: 4-Hydroxy-3, 5-dimethoxybenzoic acid	9: 3, 5-Dihydroxybenzoic acid
10: Vanillic acid	11: 4-Nitrocatechol	12: DL-Tryptophan
13: DL-Tryosine	14: Phenylalanine	15: midazole-2-formaldehyde
16: Naphthalene	17: Phenanthrene	18: Pyrene
19: Anthraquinone	20: 9-Fluorenone	21: 1-Naphthol
22:2-Napphthalenecarboxylic acid	23: Anthracene	24: Fluorene
25: Fluoranthene	26: Benzo-a-Anthracene	27: Chrysene
28: Benzo-b-Fluoranthene	29: Benzo-k-Fluoranthene	30: Perylene
31: Indeno-123cd-Pyrene	32: Benzo-ghi-Perylene	

(b)
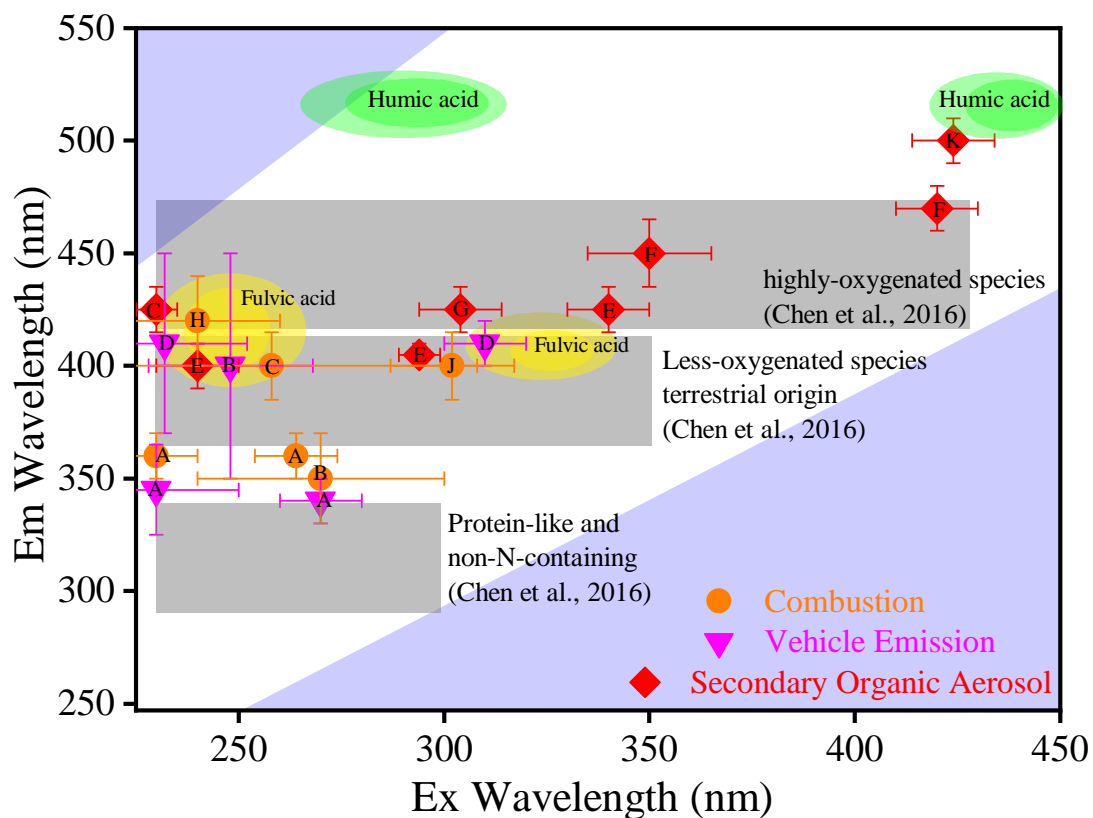
A: This study	B: Yang et al., 2022
C: Chen et al., 2020	D: Tang et al., 2020b
E: Hawkins et al., 2016	F: Bones et al., 2010
G: Lee et al., 2013	H: Mahamuni et al., 2020
J: Yan and Kim 2017	K: Powelson et al., 2014

 Figure 1. Comparison of chemical characteristics of molecules assigned to each

 fluorescence component of BrC model compounds (a) and source WSOM (b).

861

862
863
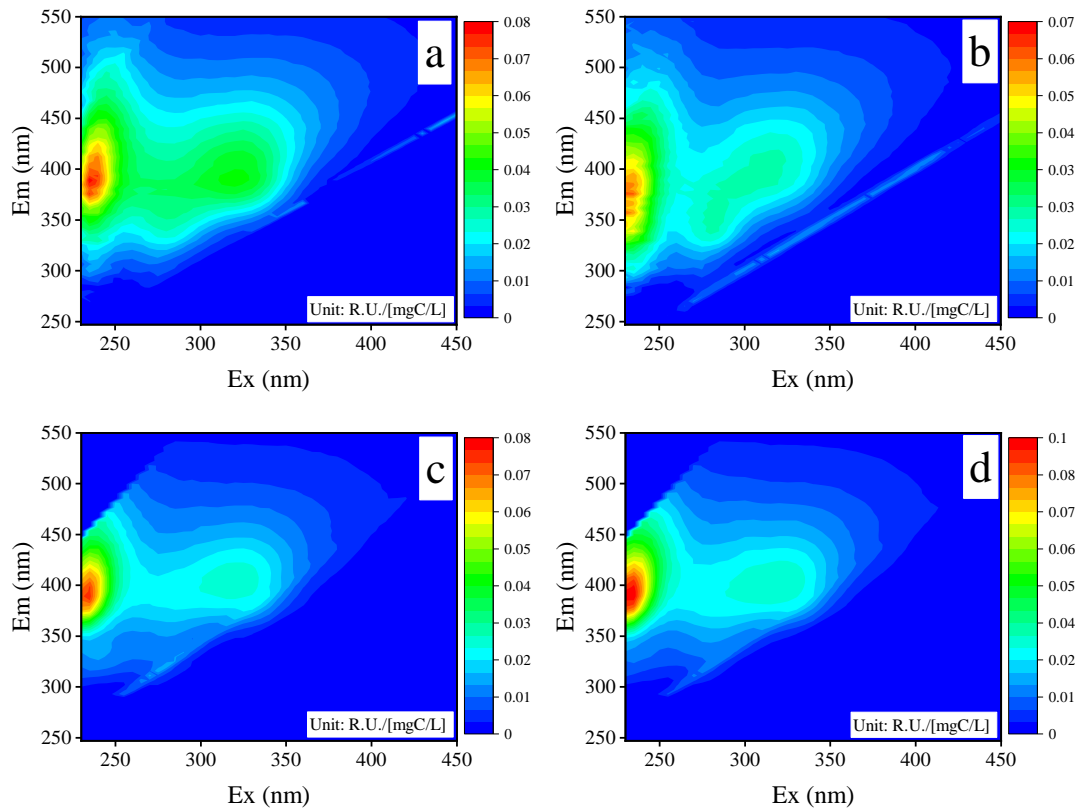
Figure 2. The 3D-EEM spectra of WSOM in atmospheric PM$_{2.5}$ samples (a:

Chuzhou (CZ); b: Guangzhou (GZ); c: GZ wet season; d: GZ dry season)

866

867
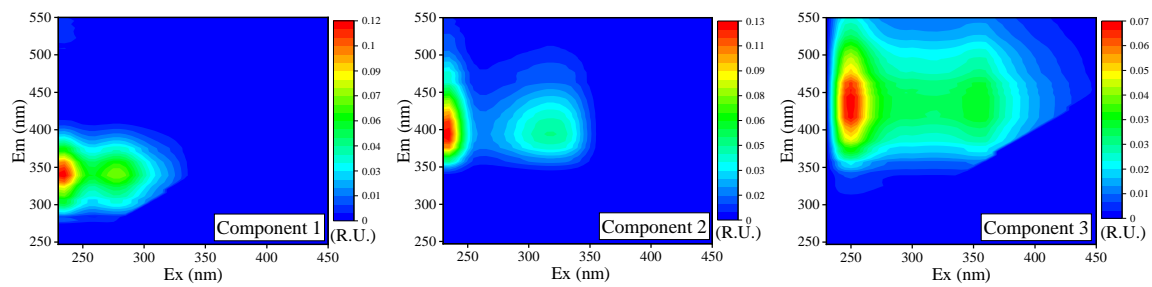
868

869 **Figure 3.** The EEM components derived from the PARAFAC model of WSOC in

870 atmospheric PM$_{2.5}$ samples collected at Chuzhou (CZ) and Guangzhou (GZ) sites.

871

872
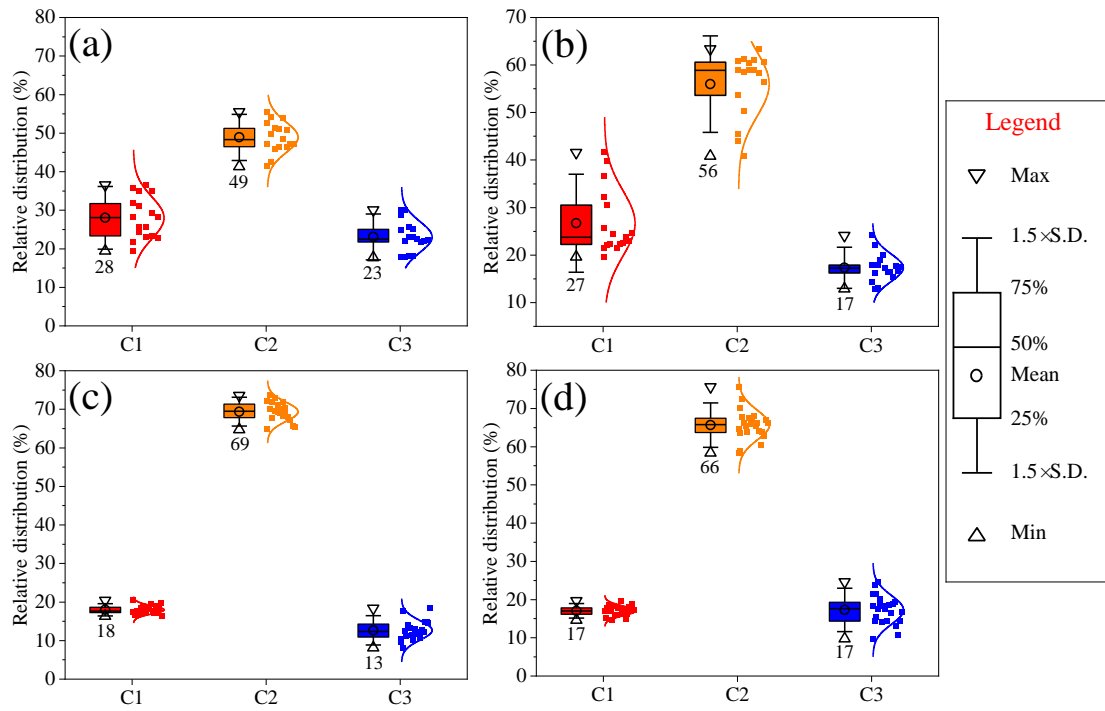
Figure 4. Relative contribution of individual fluorophores of atmospheric WSOM. (a: Chuzhou (CZ); b: Guangzhou (GZ); c: wet season of GZ; d: dry season of GZ)